Universidad de Alcalá
BIBLIOTECA

Document downloaded from the institutional repository of the University of Alcala: https://ebuah.uah.es/dspace/

This is a postprint version of the following published document:

Pacheco, M., Jurado-Sánchez, B. and Escarpa, A. (2019) 'Visible-Light-Driven Janus Microvehicles in Biological Media', Angewandte Chemie, 131(50), pp. 18185–18192. doi:10.1002/ange.201910053

Available at https://doi.org/10.1002/ange.201910053

© 2019 Wiley-VCH Verlag GmbH &Co

Universidad de Alcalá

(Article begins on next page)

This work is licensed under a

Creative Commons Attribution-NonCommercial-NoDerivatives 4.0 International License.

RESEARCH ARTICLE

Visible light driven Janus microvehicles in biological media

M. Pacheco, B. Jurado-Sánchez, [a,b]*A. Escarpa[a,b]*

Abstract: A multi-light (bio)-driven multifunctional Janus micromotor for the enhanced (bio)-detoxification of bacterial endotoxins and heavy metals is described. The micromotor is assembled using the highly biocompatible polymer polycaprolactone for the encapsulation of CdTe or CdSe@ZnS quantum dots (QDs) as photoactive materials and an asymmetric Fe_3O_4 patch for propulsion. The micromotors can be activated by visible light (470-490 nm) to propel in peroxide or glucose media at speeds of up to and 8 and 12 µm/s, respectively, by a diffusiophoretic mechanism. Efficient propulsion is observed for the first time in complex samples such as human serum blood. Such capabilities in connection with the glucose biocompatible propulsion mechanism were exploited for efficient endotoxin removal using lipopolysaccharides from *Escherichia Coli O111:B4* as model toxin. The multifunctional capabilities of the micromotors for detoxification were extended to mercury removal via cationic exchange with the CdSe@ZnS core-shell QDs. Cytotoxicity assays in HeLa cells lines demonstrated the high biocompatibility of the micromotors for future practical (bio)-detoxification applications. The results described represent a new paradigm in the use of light responsive microvehicles as active and multifunctional detoxification or even sensing platforms.

Introduction

Micromotors can be defined as self-propelled structures that can convert energy into mechanical movement to achieve complex tasks in solution.[1] Early designs compromise nanowire or tubular structures which rely on high levels of hydrogen peroxide fuel, leading to impressive analytical, environmental or biomedical applications.[2] Biocompatible propulsion schemes involve Mg or Zn micromotors with a "reactive body" activated in the presence of biological fuels (acidic gastrointestinal fluids) for *i.e.* improved therapeutics delivery or toxin neutralization.[3] Enzyme powered micromotors, propelled by low levels of biocompatible substrates such as urease or glucose, hold considerable promise for (bio)-applications, which are currently under development.[4] In a very recent report, metal organic frameworks encapsulating catalase act as highly efficient drug delivery microvehicles able to propel at the hydrogen peroxide levels present in cancer cell media, with pH modulated behavior for enhanced drug delivery.[5] Additional designs rely on the combination of micromotor structures with motile cells.[6] Cardiomyocytes have been used as "natural fuel sources" to move microdevices.[7]

Fuel-free micromotors powered by external magnetic or ultrasound fields allow for extended navigation in biological fluids.[8] Ultrasound powered gold nanowires or magnetic helices have been used as templates for coating with red-blood cell membranes (RBC) derived vesicles and/or platelets (PL) for biodetoxification of toxins and bacteria.[9] Ferrite coatings were also incorporated in magnetic propelled helices for prolonged navigation in blood.[10] Engineering single cell derived units with nanoparticles results in the so-called "cell-based" micromotors, which have been tested for theragnostic applications.[11] The native fluorescent of spirulina microalgae was exploited for the construction of magnetic micromotors for bioimaging applications.[12]

One of the recent trends in the micromotor field are directed to explore visible light as external input for autonomous propulsion.[13] Designs compromised Janus micromotors based on photoactive materials such as Cu_2O/Au, bismuth oxyiodide, TiO_2 or C_3N_4 nanomaterials.[14] Cu_2O micromotors doped with carbon nanotubes can be efficiently driven by visible-light triggered photocatalytic reaction of glucose.[15] $BiVO_4$ based micromotors can readily activate by VIS light irradiation for enhanced capture of microorganisms.[16] Yet, applications have been mostly directed to environmental remediation and only near-infrared light has been exploited for drug-triggered release schemes.[17] The promising results obtained in such fields and the high biocompatibility of the propulsion mechanism along with the collective swarming of multiple micromotors hold considerable potential to developed relevant new biomedical applications based on active micromotor movement along with detoxification capacities, leading to dynamic biomedical applications such *i.e.* enhanced detoxification or sensing.[18]

Herein we will describe, for the first time, a multi-light propelled Janus micromotor for the enhanced removal of bacterial endotoxins and heavy metals (see **Figure 1**). The micromotor can be mass-scale prepared following a simple oil-in-water emulsion procedure to encapsulate CdTe or CdSe@ZnS QDs as photoactive materials and an asymmetric Fe_3O_4 patch to induce the Janus asymmetry for propulsion into a biocompatible polycaprolactone polymeric layer. We will illustrate the fully green micromotor propulsion in glucose media upon irradiation with Vis light (470-490 nm) or low peroxide levels. Micromotor was judiciously designed to allow a close contact between the QDs with the Fe_3O_4 patch for efficient electron transfer, generating a semiconductor junction. Light exposure results a charge separation within the QDs, causing electrons to migrate from the conduction band to the Fe_3O_4 patch, creating holes for reaction with glucose or peroxide enriched media. The resulting strong photocatalytic activity induce the generation of a gradient of products around the micromotor surface, as illustrated in the time-lapse images of **Figure 1** (as compared with the negligible displacement in the absence of light). Control experiments will

[a] M. Pacheco, B. Jurado-Sánchez, A. Escarpa
Department of Analytical Chemistry, Physical Chemistry, and Chemical Engineering, University of Alcala,
Alcala de Henares, E-28871 Madrid, Spain University of Alcala, E-28807, Madrid, Spain
E-mail: beatriz.jurado@uah.es, alberto.escarpa@uah.es
[b] B. Jurado-Sánchez, A. Escarpa
Chemical Research Institute "Andres M. del Rio", University of Alcala, E-28807, Madrid, Spain

Supporting information for this article is given via a link at the end of the document

further support the proposed propulsion mechanism. The speed can be modulated by varying the light intensity and peroxide or glucose levels for future *on-demand* operations. For the first time, efficient light propulsion in serum and blood samples will be demonstrated, which to date have been only achieved in chemical propelled micromotors. This fact opens new avenues for the operation of micromotor controlled by biocompatible external sources such as light in the biomedical field. This behavior was observed both using peroxide or glucose as fuel for the generation of the gradient of products. Next, the potential of the micromotor for future biomedical applications will be illustrated for toxin and heavy metal removal. On a first example, the capacity of the outer polycaprolactone layer in connection with glucose light enhanced propulsion for efficient endotoxin removal will be illustrated using lipopolysaccharides (LPS) from *Escherichia Coli* O111:B4 as model toxin. On a second example, the multifunctional capabilities of the micromotors for simultaneous detoxification and sensing will be illustrated using mercury as model contaminant via cationic exchange with the photoactive QDs. The mercury-induced fluorescent quenching of the micromotors can be also exploited for future intracellular sensing of toxic ions and other (bio)-analytes using receptor-functionalized QDs micromotors towards theragnostic applications. Cytotoxicity assays were also performed to demonstrate the high biocompatibility of the micromotors for future practical (bio)-detoxification applications.

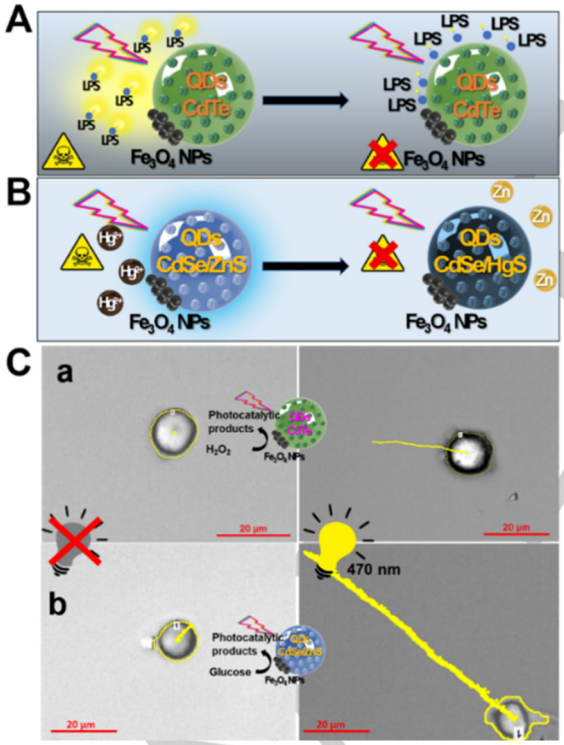

Figure 1. Schematic of the QDs/Fe_3O_4 light driven micromotors for detoxification. (A) LPS (from *Escherichia coli* O111:B4) removal by electrostatic and hydrophobic binding with the polymeric layer (polycaprolactone) of the micromotor and subsequent fluorescent quenching. (B) Mercury removal via cation exchange with Zn^{2+} ions on the QDs and subsequent fluorescent quenching. (C) Time lapse images (Taken from **Video S1**) showing the propulsion trajectories of the micromotors in 1% H_2O_2 (a) and 0.2 M glucose (b) media over 36 s without (left images) and under (right images) Vis light irradiation (470 nm).

Results and Discussion

QDs/Fe_3O_4 Vis-light (bio)-driven micromotors synthesis and propulsion mechanism. The diagram of **Figure 2A** illustrates the proposed propulsion mechanism in both peroxide and glucose media. Micromotors were synthetized using a highly versatile oil-in-water emulsion approach.[19] Such synthetic strategy allows to tailor the composition of the micromotor for the intended purpose. Emulsion was generated by mixing a sodium dodecyl sulfate solution containing the QDs and a chloroform solution with polycaprolactone [a Food and Drug Administration (FDA) approved polymer] and Fe_3O_4 nanoparticles. Droplets of the polymer containing the active nanoparticles were generated (27 ± 7 μm size). The solution was then dried overnight at room temperature to allow for polymer solidification and micromotor generation and drop size decreased to 17 ± 6 μm. **Figure S1** shows optical microscopy and scanning-electron microscopy images of several Janus micromotors confirming the final size. During such process, QDs get trapped and distributed along the micromotor body but the low miscibility of Fe_3O_4 nanoparticles in polycaprolactone promote the generation of the asymmetric patch. The close proximity of the QDs in the region containing the Fe_3O_4 nanoparticles patch allow for an efficient electron transfer between both components (via semiconductor junctions), as will be illustrated bellow with electrochemical measurements and control experiments using QDs and Fe_3O_4 micromotors. Microscopy images illustrating the Janus morphology of the micromotors are depicted in **Figure 2A**. For future biocompatibility in biomedical applications, we choose CdSe@ZnS or CdTe QDs with a bandgap energy around 2.3 eV as active elements for micromotor propulsion.

Micromotor motion can be initiated after irradiation with different light wavelengths with variable photon energies: 385 (3.2 eV), 435 (2.9 eV), 470 (2.6 eV) and 490 nm (2.5 eV). As such energies are equal or higher than the QDs bandgap, photons are absorbed by the micromotors. Next, the electrons in the valence band of QDs are excited to the conduction band, creating holes in the valence band, and in turn negative electron (e^-) are released. According to previous reports,[20] the photoexcited electrons can be transferred also to the Fe_3O_4 catalytic patch in the micromotors (via semiconductor junctions),[21] and recombine with its electronic levels, creating h^+ pairs. The positive holes can react with water and a small amount of peroxide or glucose present in the media to initiate complex radical chain reactions and produce various products such as H^+, O_2 (for peroxide) or arabinose, erythrose, formic acid, etc (for glucose).[15] This generate and accumulation of a higher concentration of photodegradative products around the micromotor surface, which further propels the micromotors. Interestingly, as illustrates in **Figure 2B** and **Video S2**, micromotors can propel efficiently in tap water, human serum and blood samples. The time lapse images demonstrate the effective

displacement and prolonged micromotor propulsion over 50 s period under light irradiation, as compared with the negligible displacement in the absence of light. Average speeds of over 4 and 3 μm/s in tap and serum samples, respectively, were observed; which reflect the viscosity and ions content in such complex samples. Micromotor propulsion was also tested in whole blood. The samples were enhanced with glucose as co-reagent from enhanced propulsion. As can be seen in **Figure 2B**, speeds of up to ~3 μm/s were obtained after light irradiation (470 nm). Surprisingly, we noted a marked displacement of the red-blood cells after light irradiation (please check **Video S2**). To check whether the micromotor propulsion is due to the fluid displacement or due to the micromotor autonomous propulsion, we perform the same experiment by replacing the micromotors with similar size polystyrene particles (20 μm). As can be seen in the images and in **Video S2**, no displacement of the PS particles is noted, which further reveals the autonomous micromotor movement in whole blood. This is the first time that light propelled micromotors based on diffusiophoretic mechanisms can efficiently operate in serum and blood samples, as only bubble-propelled micromotors have shown motion in human serum with high viscosity. This behavior was observed both using peroxide or glucose as fuel for the generation of the gradient of products.

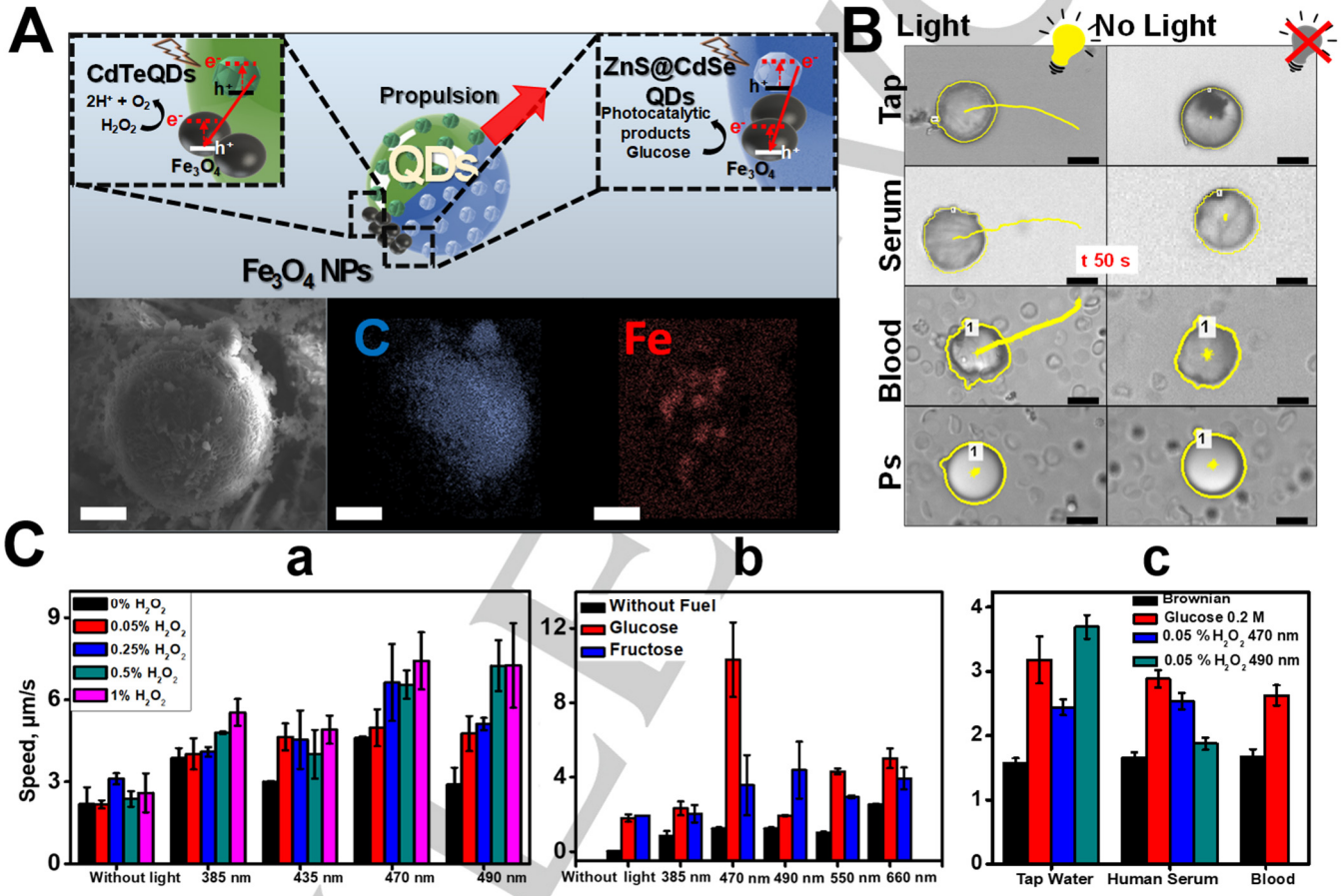

Figure 2. (A) Schematic of the propulsion mechanism of QDs/Fe_3O_4 light driven micromotors in peroxide and glucose media. Down images show the scanning-electron microscopy characterization and energy-dispersive X-ray mapping showing the morphology and element distribution on the micromotors. (B) Time lapse images (Taken from **Video S2**) showing the propulsion trajectories of the micromotors in tap water, serum and blood samples and polystyrene particles (PS) in blood samples over 50 s without (control image) and with Vis light irradiation (470 nm). (C) Influence of different light wavelengths and peroxide (a) or glucose (0.2 M) (b) concentrations on the speed of the micromotors in water and (c) serum, blood or tap water samples (at 470 nm light irradiation). Scale bars, 10 μm.

To further support the propulsion mechanism, experiments using QDs/Fe_3O_4 micromotors and, QDs or Fe_3O_4 control micromotors were performed. As can be seen in **Figure S2 A** no apparent movement or displacement is observed in micromotors containing only QDs or Fe_3O_4 nanoparticles after light exposure, with typical Brownian motion. Such results indicate that the single particles do not display any apparent photocatalytic properties alone under visible light, which reveals the critical role of the synergetic effect among both; as also reflected in the effective displacement and speed of QDs/Fe_3O_4 micromotors upon light irradiation. It should be noticed here the negligible effect of light-induced heating of the drop or a potential thermoresponsive behavior on the Brownian

motion of QDs or Fe_3O_4 micromotors and in turn, in the micromotor system. Additional chronoamperometric experiments were performed at an applied potential of +0.3 V in thin film Pt electrode to monitor the depletion of hydrogen peroxide as indicator of the photocatalytic activity of the micromotor. Measurements were performed in the presence of 0.05 % hydrogen peroxide after light irradiation (470 nm), reflecting such depletion of fuel in the presence of QDs/Fe_3O_4 micromotors (as indicated by reduction of the chronoamperometric response); whereas negligible depletion (0.05 % peroxide) is observed for control experiments, as can be seen in **Figure S2 B**. This further support the inherent photocatalytic activity of the micromotors. It should be noticed here that despite the non-conductive nature of polycaprolactone, the close contact of the QDs (trapped in the micromotor) close to the Fe_3O_4 patch allow for efficient electron transport and holes generation for the subsequent formation of the gradient of products around the micromotor, as further illustrated in control experiments.

We next studied the effect of different light intensities and glucose or peroxide concentrations upon micromotor speed (see **Figure 2C**). Under the absence of light, negligible displacement is observed (both in peroxide and glucose fueled micromotors) with speeds lower than 2 μm/s, which corresponds to Brownian motion. Upon light irradiation, effective displacement is produced, and speed increased along with peroxide concentration. Highest speeds were obtained after irradiation up to 470 nm, with velocities ranging from ~4.5 to ~8 μm/s in the absence and the presence of 1 % hydrogen peroxide, respectively. In the case of glucose, high speeds were also observed at 470 nm (up to ~12 μm/s), and some motion was also noted using fructose, yet the low efficiency in the decomposition or a lower concentration of decomposition products can be responsible for the decreased speeds. Interestingly, the speed of the micromotors can be also modulated by varying the incident light intensity from 0 to 100 mW/cm^2 (see **Figure S2 C** and **D**), with an increase in the velocity along with light intensity. This can be directly related with an increase in the incident photon flux (ø) along with intensity and hence an increase in the number of photogenerated holes and electrons pairs, leading to a faster speed of product generation according to the equation:

$$I = \emptyset \frac{hc}{\lambda}$$

where ø, h, c and λ are the incident photon flux, Planck constant, speed of light and wavelength of incident light, respectively.[14b] According to these results and the excellent biocompatibility of visible light for biological and environmental media, light irradiation at 470 nm with an intensity of 100 mW/cm^2 was selected for detoxification experiments on both modes.

Bacteria endotoxin removal with QDs/Fe_3O_4 Vis-light driven micromotors. Lipopolysaccharides or endotoxins are an integral part of the outer cell membrane of gram-negative bacteria. Such compounds are continuously released at high concentration in serum, culture media, etc. during bacteria growth and proliferation. Endotoxin possess a high toxicity at very low levels (1 ng per kg body weight and hour) if reaches bloodstream, thus its removal from parenteral preparations is of paramount significant to avoid serious health effects.[22] Most importantly, sepsis shock is mainly caused by endotoxins through activation of the immune system. Excessive release of mediators (tumor necrosis factors, interleukins) in response to endotoxins cause fatal effects such as organ failure and ultimate death. Direct removal of endotoxins from blood using polymers or magnetic nanocarriers is considered an essential tool to benefit patient's outcome.[23] Polycaprolactone nanoparticles have been also applied for endotoxin removal in water by direct binding.[24]

In a previous work from our group, we also observed that the micromotor possess a microporous structure and that endotoxins can penetrate such pores and also interact with the micromotor by adsorption.[41] Inspired by this, we apply our light propelled micromotors for *Escherichia coli O111:B4* endotoxin removal. To illustrate the monitoring of the extent of removal, FITC labelled endotoxin was used. **Figure 3A** shows time-lapse fluorescent images of a solution contaminated with 50 μg/mL of the endotoxin treated with the light-propelled micromotors (in peroxide or glucose media) at different times. As can be seen, a rapid decrease in the fluorescent intensity was noted after 15 min navigation, with a high removal rate (90 %) after 60 minutes. Prior to study the effect of interdependent parameters (light, navigation time and endotoxin concentration) and to prove the crucial role of micromotor movement endotoxin removal, we optimized the number of micromotors using a 50 μg/mL solution of LPS. The extent of removal increases along the number of micromotors from 725 to 3500 micromotors/μL, and then remained constant. **Figure 3B** reports the data (in terms of percent removal) of endotoxin "neutralization" experiments in static (without light) and after light irradiation. A direct relationship between concentration and time was noted, thus for 20 μg/mL of endotoxin, the highest removal percentage of 90% was achieved after 30 minutes navigation, whereas 60 and 70 min were needed for 50 and 100 μg/mL, respectively. In contrast, in static conditions a low removal (less than 20 %) was obtained in all cases, revealing the crucial role of micromotor movement for enhanced detoxification. In addition, low endotoxin removal (lower than 25 %) was noted in control experiments performed using micromotors under magnetic stirring and in the presence of light without any fuel (**see Figure S3 A**). This can be due to the low micromotor speed without adding any fuel or due to the inadequate mixing under magnetic stirring, as reflected in the images included in the graphic. As can be seen, most of the micromotors are sedimented at the bottom, hampering them to perform the needed motion for endotoxin removal. Similar results were observed in both peroxide and glucose media. Experiments conducted by irradiating the toxin in the absence of micromotors revealed the negligible effect of light on endotoxin degradation (results not shown). Such removal behavior was also tested using polystyrene (PS) nanoparticles (20 μm) and Fe_3O_4 nanoparticles subjected to strong Brownian motion. As can be seen in **Figure**

S3 B the extent of removal was lower than 30 % in all cases, even after 70 minutes treatment, indicating the negligible effect of such particles in the LPS removal and the superior effect of the actively moving light-propelled micromotors.

Since efficient micromotor propulsion was observed in blood, we tested the removal efficiency of the toxin in such media. Yet, as can be seen in **Figure S4**, low removal efficiencies were obtained, which can be attributed to micromotor biofouling. Also, as shown in the inset image, red-blood cells and other blood components attach to the micromotor, preventing endotoxin diffusion into the pores and the micromotor surface. Future efforts at our lab should be directed to the inclusion of a suitable anti-biofouling coating in our micromotors.

To further evaluate the potential of light propelled QDs micromotors, we perform cellular viability tests using HeLa cancer cell line with a colorimetric 3-(4,5-dimethylthiazol-2-yl)-2,5-diphenyltetrazolium bromide (MTT) assay. As shown in **Figure 3D**, the endotoxin exhibits high toxicity, with a cell viability of over 19 %. The free QDs were moderately toxic, with 50 % cell viability (data not shown). Yet, when encapsulated in the micromotors, almost 100 % cell viability was obtained due to the polycaprolactone coating act as shield, avoiding the toxicity. Such results also indicate the excellent compatibility of the micromotors (along with a non-harmful propulsion mechanism) for future biomedical applications.

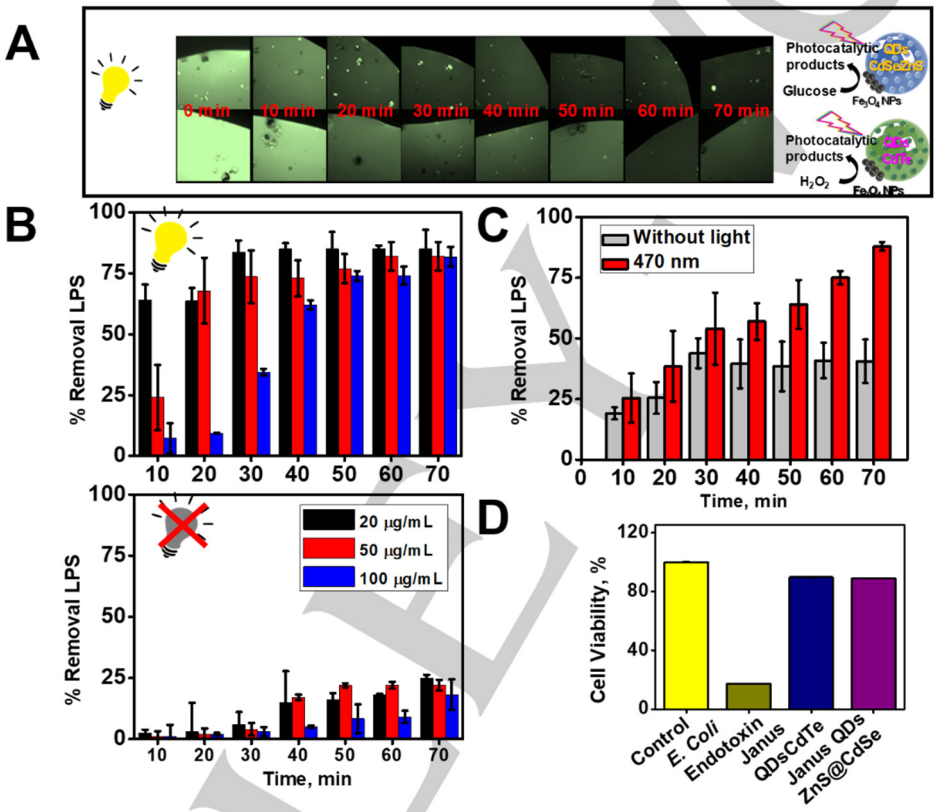

Figure 3. *Escherichia coli O111:B4* (FITC labelled) endotoxin removal by CdSe@ZnS/Fe_3O_4 Vis-light driven micromotors (A) Time-lapse fluorescent microscopy images showing the native fluorescent decay of the endotoxin solution (50 µg/mL) after micromotor navigation at different times in glucose and peroxide media (B) Study of removal percentage over time of different endotoxin concentration in peroxide media with (top) and without (bottom) light (470 nm). (C) Effect of interdependent parameters (light and navigation time) in glucose media (50 µg/mL of endotoxin). (D) Cellular viability MTT assay: cytotoxicity of free endotoxin and loaded Janus micromotors and against HeLa cells after 24 hours of incubation. Error bars were estimated as three times the standard deviation (n = 3).

Heavy metal detoxification and sensing with QDs/Fe_3O_4 Vis-light driven micromotors. Figure 4A shows a schematic of the heavy metal removal principle, where we choose Hg^{2+} ions as model to prove the concept. Based on previous knowledge from our group, such exchange can result in a selective quenching of the fluorescent the QDs, which can be exploited as a warning system for the presence of such toxic ion and other similar analytes for future theragnostic applications.[50] To develop such strategy, we inspired in the cation-exchange capacity of Cd and Zn based QDs, which is widely exploited for the generation of novel nanostructures.[25] Thus, the photo responsive QDs can also interact with Hg^{2+}, resulting in a cationic exchange replacement of Cd^{2+} to generate HgTe QDs. To test this assumption, we place a fix number of micromotors (430 micromotors/μL) in 1 mL of Hg^{2+} contaminated solutions, which was irradiated with light (470 nm) for 5 min. As can be seen in **Figure 4A**, a, the initial strong fluorescent of the micromotor (corresponding to the QDs) is quenched after 10 s navigation. According to the Gibbs free energy equation, $\Delta G^0 = -RTlnK_{ps}$, the lower the solubility constant (K_{ps}), the more positive is the free energy. Due to the solubility constants of HgTe or HgS are much lower than that of CdTe or ZnS, cation-exchange generation is favored for highly efficient heavy metal removal.[26] Interestingly, as can be seen in **Video S3**, micromotor motion stop after 10 s navigation in the contaminated solution, due to the bandgap of the generated Hg-based QDs is 3.6 eV, which is higher than the incident photon energy (2.6 eV), preventing thus electron promotion. This finding indicates the proposed ion-exchange mechanisms. To provide further evidence for the formation of such Hg QDs, we dissolve the micromotor body in chloroform before and after Hg^{2+} removal experiments and perform HRTEM and UV-Vis characterization of the released contents. After micromotor navigation in Hg^{2+} contaminated solutions, the QDs size change from 2.4 (CdTe) to 4.0 nm (HgTe) (see **Figure 4A, b**) in agreement with the higher atomic size of Hg vs Cd. Apparent changes are also observed in the UV-Vis spectra and TAUC plots of both solutions (See **Figure 4A c-d**), with a blue shift after Hg^{2+} removal experiments, suggesting a change in the electronic transitions and thus in the physical properties.

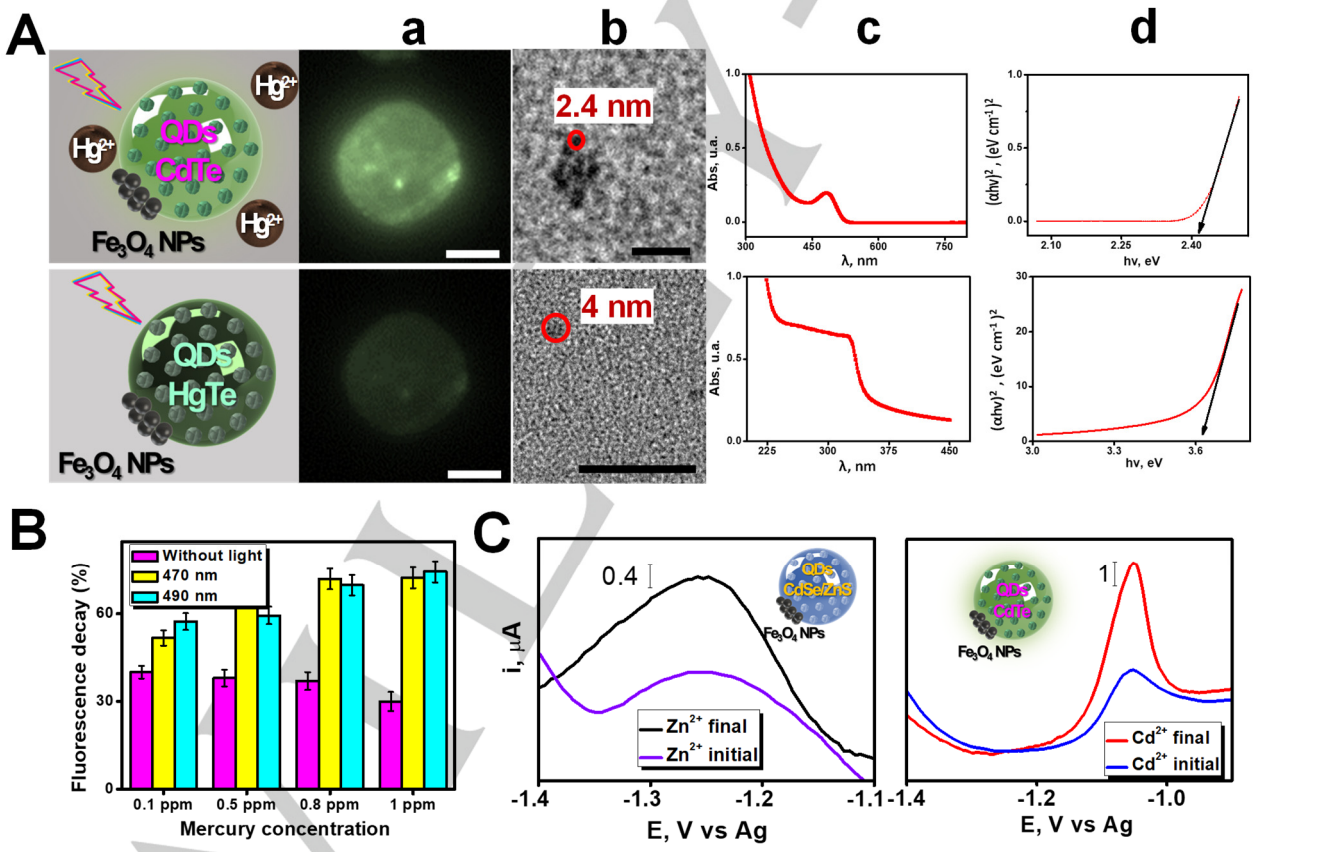

Figure 4. (A) Schematic of Hg^{2+} ions removal by CdTe or CdSe@ZnS QDs loaded/Fe_3O_4 Vis-light driven Janus micromotors via cationic exchange: a) Fluorescent microscopy images (taken from **Video S3**) illustrating the original CdTe QDs fluorescence (top) and the fluorescent quenching of the micromotors by Hg^{2+} ions (bottom); b) HRTEM images of CdTe QDs (top) and HgTe QDs released from the micromotors after mercury exchange (bottom); c, d) corresponding UV/Vis spectra and TAUC plot of CdTe (top) and HgTe (bottom) QDs. (B) Effect of interdependent parameters on mercury removal. (C) Stripping voltammograms showing the amount of Zn^{2+} or Cd^{2+} released from the micromotors after Hg^{2+} removal. Scale bars, 20 nm (HRTEM) and 10 μm (SEM).

The crucial role of micromotor movement was tested by performing experiments under static (in the absence of light) and moving (with light irradiation) conditions using increasing concentrations of Hg^{2+} contaminated solutions (0.1-1 ppm). Experiments were performed in 1 mL contaminated solutions containing 430 micromotors/μL (which was previously optimized, results not shown). The extent of removal was monitored indirectly through the extent fluorescent decay of the micromotor (n=50 at each condition); similar to QDs based sensors.[27] Fluorescent decay will increase along with Hg^{2+} concentration, thus a higher decays where associated with higher mercury removal percentage. A 75% percent of fluorescent decay was obtained with moving micromotors, whereas 30% decay was observed in static conditions in all cases. The enhanced micromotor movement increase the rate of Hg^{2+}-micromotor collisions, resulting in a greatly improved removal percentages as compared with static conditions. Additional experiments were performed to monitor the removal of Hg^{2+} (1 ppm) by anodic stripping voltammetry using carbon screen-printed electrodes. Almost quantitative removal was observed after treatment with 430 and 2000 micromotors/μL in the presence of light, as shown in **Figure S5.** Please note that CdTe QDs were initially selected as model to prove the concept of simultaneous removal and sensing. Such nanoparticles can be replaced for more biocompatible units more useful in practical applications, indeed, similar results were obtained for CdSe@ZnS loaded micromotors. The efficiency of the micromotor along with the high biocompatible propulsion mechanism hold considerable promise for future environmental remediation and on-body detoxification applications. Yet, as we are concerned with possible risk associated with the release of Cd^{2+} or Zn^{2+} ions after the cationic exchange process we measure the content of such ions in the solution by anodic stripping voltammetry (see **Figure 4C**), which were found to be 196 and 82 μg/L, respectively. Zn^{2+} is a non-toxic element essential for human health and will not cause any harmful effects at the concentration previously reported. Please also note the recommended dietary allowance for zinc is 10 mg/day for adults and 3 mg/day for infants, which is 120 and 40 times higher than that released for the micromotor, further revealing the low toxicity of the by-product.[28] Thus, for future practical applications, CdSe@ZnS micromotors, which do not release potential toxic products, can be used. Yet, the ability of selective fluorescent quenching associated with the Hg removal hold considerable promise as a novel proof-of-concept application of light driven micromotors for biodetoxification. The concept can be extended to the detection of other analytes relevant in many diseases using receptor functionalized QDs loaded micromotors with selective adsorption properties without the release of another ions.

Conclusion

In conclusion, we have described the synthesis of a highly biocompatible multi-light propelled Janus micromotor for endotoxin and heavy metal removal. Fully biocompatible and non-harmful VIS light is used as external trigger for micromotor propulsion. In addition, the combination of a biocompatible polymer with ability to adsorb toxins along with photoactive QDs with exchange capacity capabilities leads to a powerful platform for future biomedical or environmental applications of light driven micromotors not described to date. Most importantly, micromotor propulsion along with the inherent catalytic activities allow for improved and efficient movement in biocompatible glucose media. Such bio-compatible propulsion mechanism was exploited for enhanced detoxification of deadly toxins. In a second application, the micromotor was further exploited for mercury removal. The concept can be extended for the simultaneous enhanced removal or even of a myriad of toxins or bioanalytes (both in the intracellular and extracellular environment), where the cooperative action of a swarming of light propelled micromotors in connection with receptor functionalized quantum dots can add new dimensions to theragnostic approaches. Another fundamental new result is the demonstration, for the first time, of the motion of diffusiophoretic micromotor propulsion in raw human serum (both using peroxide and glucose as fuel) and blood (using glucose as fuel), which to date has been only achieved in chemical propelled micromotors. This fact opens new avenues for the operation of micromotor controlled by biocompatible external sources such as light in the biomedical field. Yet, low removal efficiencies were obtained in blood due to attachment of red-blood cells and other blood components to the micromotor, preventing endotoxin diffusion into the pores and the micromotor surface. Future efforts at our lab should be directed to the inclusion of a suitable anti-biofouling coating in the micromotors. The micromotors possess excellent biocompatibility with cell viability of almost 100 % in HeLa cell proliferation assays. The new proof-of-concept work is still at an early stage and requires further improvements before their potential uses (such as combination with multiple light sources such as NIR or VIS) such as design of biomedical technology to address the limitation of light penetration beyond the dermis. Yet, it opens the door to the use light-responsive microvehicles as an active biodetoxification or in-vivo sensing platforms.

Acknowledgements

M. Pacheco acknowledges the FPU fellowship received from the Spanish Ministry of Education (FPU 16/02211). B. J-S acknowledges support from the Spanish Ministry of Science, Innovation and Universities (RYC-2015-17558, co-financed by EU) and from the University of Alcala (CCG2018/EXP-018). AE acknowledges financial support from the Spanish Ministry of Science, Innovation and Universities (CTQ2017-86441-C2-1-R) and the TRANSNANOAVANSENS program (S2018/NMT-4349) from the Community of Madrid. Authors thanks Isabel Trabado and CAI from the university of Alcala for help during cell viability MTT assays.

Keywords: Micromotors • light • detoxification • toxin• heavy metal

[1] [1] a) G. A. Ozin, I. Manners, S. Fournier-Bidoz, A. Arsenault, *Adv. Mater.* 2005, *17*, 3011-3018; b) S. Sanchez, M. Pumera, *Chem. Asian J* 2009, *4*, 1402-1410; c) A. A. Solovev, Y. Mei, E. Bermúdez Ureña, G. Huang, O. G. Schmidt, *Small* 2009, *5*, 1688-1692; d) S. J. Ebbens, J. R. Howse, *Soft Matter* 2010, *6*, 726; e) J. Wang. Nanomachines: Fundamentals and Applications; Wiley-VCH: Weinheim, 2013.

[2] a) B. Jurado-Sanchez, J. Wang, *Environ. Sci. Nano* **2018**; b) L. Kong, J. Guan, M. Pumera, *Curr. Opin. Electrochem.* **2018**, *10*, 174-182; c) B. J. Nelson, I. K. Kaliakatsos, J. J. Abbott, *Ann. Rev. Biomed. Eng.* **2010**, *12*, 55-85.

[3] a) C. Chen, E. Karshalev, J. Li, F. Soto, R. Castillo, I. Campos, F. Mou, J. Guan, J. Wang, *ACS Nano* **2016**, *10*, 10389-10396; b) X. Wei, M. Beltrán-Gastélum, E. Karshalev, B. Esteban-Fernández de Ávila, J. Zhou, D. Ran, P. Angsantikul, R. H. Fang, J. Wang, L. Zhang, *Nano Lett.* **2019**, *19*, 1914-1921; c) M. Zhou, T. Hou, J. Li, S. Yu, Z. Xu, M. Yin, J. Wang, X. Wang, *ACS Nano* **2019**, *13*, 1324-1332; d) Z. Wu, J. Li, B. Esteban-Fernández de Ávila, T. Li, W. Gao, Q. He, L. Zhang, J. Wang, *Adv. Function. Mater.* **2015**, *25*, 7497-7501.

[4] T. Patiño, X. Arqué, R. Mestre, L. Palacios, S. Sánchez, *Acc. Chem. Res.* **2018**, *51*, 2662-2671.

[5] S. Gao, J. Hou, J. Zeng, J. J. Richardson, Z. Gu, X. Gao, D. Li, M. Gao, D.-W. Wang, P. Chen, V. Chen, K. Liang, D. Zhao, B. Kong, *Adv. Funct. Mater.* **2019***, 29, 1808900*.

[6] a) H. Xu, M. Medina-Sánchez, V. Magdanz, L. Schwarz, F. Hebenstreit, O. G. Schmidt, *ACS Nano* **2018**, *12*, 327-337; b) M. M. Stanton, B.-W. Park, A. Miguel-López, X. Ma, M. Sitti, S. Sánchez, *Small* **2017**, *13*, 1603679.

[7] B. J. Williams, S. V. Anand, J. Rajagopalan, M. T. A. Saif, *Nat. Commun.* **2014**, *5*, 3081.

[8] a) S. Tottori, L. Zhang, F. Qiu, K. K. Krawczyk, A. Franco-Obregón, B. J. Nelson, *Adv. Mater.* **2012**, *24*, 811-816; b) D. Schamel, A. G. Mark, J. G. Gibbs, C. Miksch, K. I. Morozov, A. M. Leshansky, P. Fischer, *ACS nano* **2014**, *8*, 8794-8801; c) L. Ren, W. Wang, T. E. Mallouk, *Acc. Chem. Res.* **2018**, *51*, 1948-1956.

[9] a) B. Esteban-Fernández de Ávila, W. Gao, E. Karshalev, L. Zhang, J. Wang, *Acc. Chem. Res.* **2018**, *51*, 1901-1910; b) Z. Wu, T. Li, W. Gao, T. Xu, B. Jurado-Sánchez, J. Li, W. Gao, Q. He, L. Zhang, J. Wang, *Adv. Funct. Mater.* **2015**, *25*, 3881-3887; c) B. Esteban-Fernández de Ávila, P. Angsantikul, D. E. Ramírez-Herrera, F. Soto, H. Teymourian, D. Dehaini, Y. Chen, L. Zhang, J. Wang, *Sci. Robot.* **2018**, *3,* eaat0485; d) J. Li, P. Angsantikul, W. Liu, B. Esteban-Fernandez de Avila, X. Chang, E. Sandraz, Y. Liang, S. Zhu, Y. Zhang, C. Chen, W. Gao, L. Zhang, J. Wang, *Adv. Mater.* **2018**, *30,* 1704800-1704808.

[10] P. L. Venugopalan, R. Sai, Y. Chandorkar, B. Basu, S. Shivashankar, A. Ghosh, *Nano Lett.* **2014**, *14*, 1968-1975.

[11] a) J. Shao, M. Xuan, H. Zhang, X. Lin, Z. Wu, Q. He, *Angew. Chem. Int. Ed.* **2017**, *56*, 12935-12939; b) Z. Wu, T. Li, J. Li, W. Gao, T. Xu, C. Christianson, W. Gao, M. Galarnyk, Q. He, L. Zhang, J. Wang, *ACS nano* **2014**, *8*, 12041-12048; c) Z. Wu, B. Esteban-Fernández de Ávila, A. Martín, C. Christianson, W. Gao, S. K. Thamphiwatana, A. Escarpa, Q. He, L. Zhang, J. Wang, *Nanoscale* **2015**, *7*, 13680-13686.

[12] X. Yan, Q. Zhou, M. Vincent, Y. Deng, J. Yu, J. Xu, T. Xu, T. Tang, L. Bian, Y.-X. J. Wang, K. Kostarelos, L. Zhang, *Sci. Robot.* **2017**, *2*, eaaq1155.

[13] a) R. Dong, Y. Cai, Y. Yang, W. Gao, B. Ren, *Acc Chem Res* **2018**, *51*, 1940-1947; b) S. Palagi, A. G. Mark, S. Y. Reigh, K. Melde, T. Qiu, H. Zeng, C. Parmeggiani, D. Martella, A. Sanchez-Castillo, N. Kapernaum, F. Giesselmann, D. S. Wiersma, E. Lauga, P. Fischer, *Nat Mater* **2016**, *15*, 647; c) R. María Hormigos, B. Jurado-Sánchez, A. Escarpa, *Angew Chem Int Ed* **2019**, *58*, 3128-3132.

[14] a) R. Dong, Y. Hu, Y. Wu, W. Gao, B. Ren, Q. Wang, Y. Cai, *J Am Chem Soc* **2017**, *139*, 1722-1725; b) B. Jang, A. Hong, H. E. Kang, C. Alcantara, S. Charreyron, F. Mushtaq, E. Pellicer, R. Buchel, J. Sort, S. S. Lee, B. J. Nelson, S. Pane, *ACS Nano* **2017**, *11*, 6146-6154; c) D. Zhou, Y. C. Li, P. Xu, N. S. McCool, L. Li, W. Wang, T. E. Mallouk, *Nanoscale* **2017**, *9*, 75-78; d) E. O'Neel-Judy, D. Nicholls, J. Castaneda, J. G. Gibbs, *Small* **2018**, 1801860-1801866; e) K. Villa, C. L. Manzanares Palenzuela, Z. Sofer, S. Matějková, M. Pumera, *ACS nano* **2018**, *12*, 12482-12491.

[15] Q. Wang, R. Dong, C. Wang, S. Xu, D. Chen, Y. Liang, B. Ren, W. Gao, Y. Cai, *ACS Appl. Mater. Interfac.* **2019**, *11*, 6201-6207.

[16] K. Villa, F. Novotný, J. Zelenka, M. P. Browne, T. Ruml, M. Pumera, *ACS nano* **2019**, *13*, 8135-8145.

[17] a) Z. Wu, X. Lin, Y. Wu, T. Si, J. Sun, Q. He, *ACS nano* **2014**, *8*, 6097-6105; b) Q. Rao, T. Si, Z. Wu, M. Xuan, Q. He, *Sci. Rep.* **2017**, *7*, 4621.

[18] J. Wang, Z. Xiong, J. Zheng, X. Zhan, J. Tang, *Acc. Chem. Res.* **2018**, *51*, 1957-1965.

[19] a) B. Jurado-Sánchez, M. Pacheco, J. Rojo, A. Escarpa, *Angew. Chem. Int. Ed.* **2017**, *56*, 6957-6961; b) W. Gao, M. Liu, L. Liu, H. Zhang, B. Dong, C. Y. Li, *Nanoscale* **2015**, *7*, 13918-13923.

[20] a) Q. Zhang, R. Dong, Y. Wu, W. Gao, Z. He, B. Ren, *ACS Appl. Mater. Interfac.* **2017**, *9*, 4674-4683; b) R. Dong, Q. Zhang, W. Gao, A. Pei, B. Ren, *ACS nano* **2016**, *10*, 839-844.

[21] a) I. A. Digdaya, G. W. P. Adhyaksa, B. J. Trześniewski, E. C. Garnett, W. A. Smith, *Nat Commun* **2017**, *8*, 15968; b) G. Xi, B. Yue, J. Cao, J. Ye, *Chem-Eur J* **2011**, *17*, 5145-5154.

[22] a) F. B. Anspach, *J. Biochem. Biophys. Methods* **2001**, *49*, 665-681; b) J. C. Kagan, *Science* **2013**, *341*, 1184-1185.

[23] I. K. Herrmann, M. Urner, S. Graf, C. M. Schumacher, B. Roth-Z'graggen, M. Hasler, W. J. Stark, B. Beck-Schimmer, *Adv. Healthc. Mater.* **2013**, *2*, 829-835.

[24] M. L. Donnell, A. J. Lyon, M. R. Mormile, S. Barua, *Nanotechnol.* **2016**, *27*, 285601.

[25] D. H. Son, S. M. Hughes, Y. Yin, A. P. Alivisatos, *Science* **2004**, *306*, 1009-1012.

[26] a) B. Jurado-Sánchez, A. Escarpa, J. Wang, *Chem. Commun.* **2015**, *51*, 14088-14091; b) A. Jaiswal, S. S. Ghsoh, A. Chattopadhyay, *Langmuir* **2012**, *28*, 15687-15696.

[27] B. B. Campos, M. Algarra, B. Alonso, C. M. Casado, J. C. G. Esteves da Silva, *Analyst* **2009**, *134*, 2447-2452.

[28] P. Trumbo, A. A. Yates, S. Schlicker, M. Poos, *J. Am. Diet. Assoc.* **2001**, *101*, 294–301

Entry for the Table of Contents

Layout 1:

RESEARCH ARTICLE

VIS light driven micromotors shows enhanced propulsion in peroxide and glucose media for detoxification of bacterial endotoxins and heavy metals.

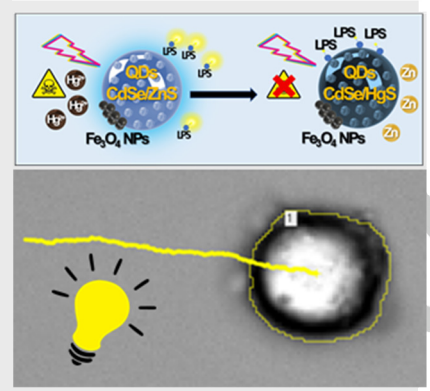

*M. Pacheco, B. Jurado-Sánchez,*A. Escarpa**

Page No. – Page No.

Visible light driven Janus microvehicles in biological media

WILEY-VCH